Decode and Forward Coding Scheme for Cooperative Relay NOMA System with Cylindrical Array Transmitter

Samuel Tweneboah-Koduah[1]
Department of Computer and Electrical Engineering
University of Energy and Natural Resources
Sunyani, Ghana

Emmanuel Ampoma Affum[2]
Department of Telecommunication Engineering
University of Science and Technology
Kumasi, Ghana

Kingsford Sarkodie Obeng Kwakye[3]
Department of Telecommunication Engineering
University of Science and Technology
Kumasi, Ghana

Owusu Agyeman Antwi[4]
Department of Telecommunications Engineering
Ghana Communication Technology University
Accra, Ghana

Abstract—The Non-Orthogonal Multiple Access (NOMA) technique has enormous potential for wireless communications in the fifth generation (5G) and beyond. Researchers have recently become interested in the combination of NOMA and cooperative relay. Even though geometric-based stochastic channel models (GBSM) have been found to provide better, practical, and realistic channel properties of massive multiple-input multiple-output (mMIMO) systems, the assessment of Cooperative Relay NOMA (CR-NOMA) with mMIMO system is largely based on correlated-based stochastic channel model (CBSM). We believe that this is a result of computational difficulties. Again, not many discussions have been done in academia about how well CR-NOMA systems perform when large antenna transmitters with the GBSM channel model are used. As a result, it is critical to investigate the mMIMO CR-NOMA system with the GBSM channel model that takes into account channel parameters such as path loss, delay profile, and tilt angle. Moreover, the coexistence of large antenna transmitters and coding methods requires additional research. In this research, we propose a two-stage, three-dimension (3D) GBSM mMIMO channel model from the 3GPP, in which the transmitter is modelled as a cylindrical array (CA) to investigate the efficiency of CR-NOMA. By defining antenna elements placement vectors using the actual dimensions of the antenna array and incorporating them into the three-dimension (3D) channel model, we were able to increase the analytical tractability of the 3D GBSM. Bit-error rates, achievable rates, and outage probabilities (OP) are investigated utilizing the decode-and-forward (DF) coding method: the results are compared with that of a system using the CBSM channel model. Despite the computational difficulties of the proposed GBSM system, there is no difference in performance between CBSM and GBSM.

Keywords—*CR-NOMA; 3D GBSM; DF coding scheme; Cylindrical Array (CA); cooperative relay*

I. INTRODUCTION

One of the major hurdles for future wireless communication systems is to facilitate large data traffic whilst maintaining reasonable communication latency [1]–[3]. This is due to the development of information and communication applications and a rapidly expanding user base. It also requires concurrent access to various network resources from anywhere and at any time while maintaining a good quality of service.
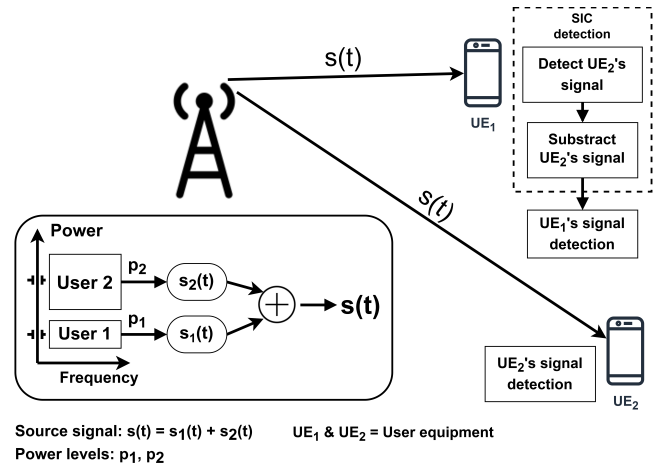

Fig. 1. NOMA System Architecture for Downlink Communication.

In a cellular system where the channel conditions vary for various users due to the near-far effect, Nonorthogonal multiple access (NOMA) provides performance improvement regarding the trade-off between the system's capacity and user fairness [4]–[7]. *Fig.* 1 Figure 1 illustrates the NOMA system architecture for downlink (DL) communication. According to the NOMA concept in the power domain, users share the same resource block such as frequency, code or time. The users, however, are assigned different power levels per the channel conditions. Users with a poor channel are given more power than those with a good channel state. The data signal of various users in the NOMA system is added together by using superposition coding into a single data signal that is transmitted to all users within the network. This will be seen in later sections of this work. At the destination, the users employ successive interference cancellations to mitigate interference and recover individual data signals. NOMA, which has been

incorporated into the new 5G standard, is a promising method that is anticipated to meet the requirements and also deliver a greater spectrum efficiency [6], [7].

Given the incredibly high number of IoT devices enabled by 5G (such as Smart Cities or Autonomous Vehicles), this trait is important in situations where the spectrum is limited. Users who are nearer the transmitter utilize lower transmit powers, but users who are farther away need greater transmit powers. As a result, NOMA employs these attributes to distinguish between signals since transmissions from various users who share the same spectrum have varying received power levels. Naturally, in addition to the near-far issue, fading and power regulation are other elements that cause variances in the received power levels of users. These characteristics are also taken into consideration by the NOMA receiver. When using NOMA, a user receiving the superposition broadcast with its signal delivered at a lower power level decodes the stronger signal components of other users and then cancels them out. This allows for a considerable spectral efficiency increase over standard orthogonal multiple access [8]. Some of the major technologies that enable 5G communications to achieve the initial targets in terms of throughput, spectrum efficiency, and network capacity are massive multiple-input, multiple output (mMIMO), millimeter-wave (mmWave) Communications, Cooperative relay NOMA (CR-NOMA), and so on [9], [10].

The advantage of mmWave, which uses carrier frequencies of about 60 GHz, is that it has a substantially larger channel coherence bandwidth but also has significantly higher path loss. Additionally, the relatively short wavelength of mmWave makes it easier to deploy mMIMO since it allows for smaller antennas and closer spacing between mMIMO antenna components (typically 3 to 4 wavelengths for the signals in adjacent antennas to be uncorrelated).

Recent works have seen the integration of NOMA and different transmission techniques, such as mMIMO, mmWave, block transmission techniques, and cooperative-relay communication. This is to achieve better system performance. Cooperation among network users is crucial in wireless communication since it reduces fading effect, increases capacity, and broadens the coverage area. Cooperative communication occurs when a node works with the source to forward data to the destination as indicated in *Fig.* 2 and 3. Two types of cooperation, namely cooperation among NOMA users and cooperation via specialized relays, can be employed to create cooperative diversity in the NOMA system. By utilizing idle users to relay data to other users, the previous method is used to increase the data rate and data dependability for the weak users. The latter is used to serve cell edge NOMA customers effectively within a network and to increase wireless network coverage [11].

II. LITERATURE REVIEW

1) Channel Models for 5G Massive MIMO: A channel model is a mathematical depiction of the impacts of a communication channel used to transmit wireless communications. The channel model can reflect the signal's power loss as it passes via the wireless link. There are two types of channel models that are typically used to evaluate the performance of 5G wireless communication systems: correlation-based

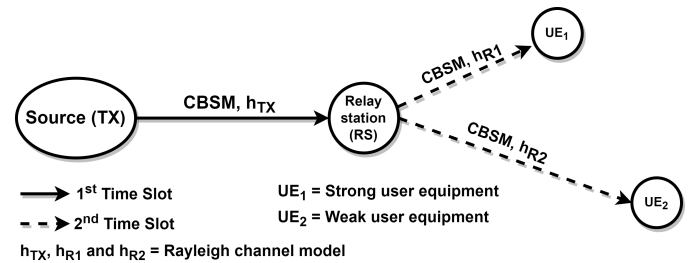stochastic models (CBSMs) and geometry-based stochastic models (GBSMs) [12].

Fig. 2. Downlink cooperative-Relay NOMA Network with CBSM Channel Model.

Table I gives further details of these channel models and their applications. The former is less accurate and is mostly used to study the theoretical performance of MIMO systems. The exactitude of a true MIMO system, on the other hand, is limited, and simulating wireless channels with the nonstationary phenomenon and wavefront effects is difficult [12], [13]. GBSM, on the other hand, has more processing complexity, but it can accurately represent actual channel characteristics and is ideally adapted for mMIMO channel estimation [12].

For performance improvements and evaluation, GBSM combines channel features such as angle of arrivals, delay profile, tilt angle, path-loss, and so on into the channel models [12], [14]–[16].

2) CR-NOMA with CBSM Channel Model: As explained previously, the effectiveness of CR-NOMA has been thoroughly investigated using a variety of network coding methods. However, the vast majority of CR-NOMA performance assessments are only based on CBSM, which is mainly used for theoretical MIMO channel analyses. Cooperation among devices in a network has been studied in numerous literature, where some network nodes act as a relay to other devices by using network coding strategies. The network coding strategies improve system performance and allow the far or network edge users to improve their quality of services. For instance, [17] investigated network coding techniques such as amplify-and-forward and decode-and-forward. One of the most well-known relaying protocols is Decode-and-forward (DF). In this protocol, a relay decodes the message from a source and resends the decoded symbols to a destination. DF MIMO relay systems' transmission strategy and performance analyses have been done in [18]. Additionally, the compress-and-forward (CF) and compute-and-forward (CpF) techniques have been examined in [19], [20] and [21]–[24], respectively. The above coding schemes were used to analyze resource allocation optimization in [25]–[30].

CR-NOMA using MIMO as well as mMIMO have been investigated in [31], [32] to increase system spectral efficiency and lessen difficulties in acquiring channel state information (CSI). The applicability of relay to mMIMO NOMA has been researched by the authors of [32]. However, CBSM was the foundation of the analyses with mMIMO cooperative relay NOMA. According to [12], the authors' circular array at the transmitter (TX) can not be considered as a typical antenna array arrangement for mMIMO systems.

TABLE I. COMPARISON OF MIMO CHANNEL MODELS [12], [15]

Specifications	GBSM	CBSM
Suitable environments	• Scatters are stochastically distributed between link ends. • Realistic analysis of physical propagation environment.	• Describes channel characteristic by correlation matrices instead of propagation parameters.
Benefits	• Suitable for simulation of geometric path using numerous random parameters. • High degree of random parameters yields high accuracy. • Suitable for adaptive antenna application.	• Serves as a better calibration (channel) mode. • Suitable for link-level simulation. • Better calibration model. • Suitable for evaluating theoretical performance of MIMO system due to low complexity.
Limitation	• High complexity due to high degree of parameter randomness.	• Simple and computational efficient. • Inaccurate for realistic MIMO system analysis. • Not suitable for system-level simulation due to over simplification of channel model.
Features	• Distinctive random variables of multiple subpath of a cluster path. • Correlation properties depend on spatial characteristics and antenna array configuration.	• Correlation properties depend of channel matrices depends on Doppler and spatial filtering. • Describes channel characteristic by correlation matrices instead of propagation parameters.
Classification	• 2D Models (Parabolic and Elliptical) • 3D Models (Ellipsoid, 5G channel and Twin-cluster) • Saleh-Valenzuela model	• I.I.D. Rayleigh fading channel • Racian channel model • Kronecker model • Mutual coupling model (Weichselberge model and Virtual channel representation)
Application	• 5G, vehicle-to-vehicle (V2V) communication, high-speed train (HDT) communication, unmanned aerial vehicle (UAV) communication, etc.	• Low frequency, low speed applications.

A. Motivation

According to research, CBSM [23], [33]–[36] is the only focus of the approaches and analyses utilized to enhance CR-NOMA system performance. Due to nonstationary phenomena and spherical effects, CBSM is used for theoretical study and has lower accuracy for real-world mMIMO systems [12], [37]. *Table* I provides a comparative study of CBSM and GBSM that clearly outlines the drawbacks of the CBSM channel model. GBSM on other hand provides accurate and realistic channel characteristics for the mMIMO system. In this regard, the authors in [31] have, as far as we can determine, used GBSM to examine CR-NOMA performance based on the Saleh-Valenzuela channel model. The authors considered the channel for beamforming analysis without network coding strategies. Again, a user relay rather than a specialized relay station was the focus of their investigation. The purpose of this study is to fill in the gap in the literature on CR-NOMA related to the adoption of the 3GPP's 3D GBSM channel model with large antenna transmitters like cylindrical antenna array (CA), as well as its implications for wireless communications. To meet future demands of wireless communication technologies

the paper addresses the following research challenges: 1) What are the effects of large antenna transmitters such as CA on the performance of mMIMO CR-NOMA systems when the communication links from the transmitter to users are modeled as 3D GBSM channel model? 2) How will mMIMO CR-NOMA performance be impacted by the combination of large antenna transmitters, 3D GBSM channel models, and coding schemes on outage probability, achievable rate, and bit-error rate (BER)?

B. Contribution

By taking into account a two-stage downlink network model system with a dedicated relay, we can address the challenges above. We use 3GPP and WINNER+ models, which adhere to the GBSM strategy, see [38], [39] for more information [14], [40]. Therefore, according to [41], defining propagation paths in azimuth does not enhance performance. By combining a space-time signal with scanning acceleration, CA may be utilized to lessen clutter and enables concentrated beams in any horizontal direction [14]. By defining the antenna element placement vector using its physical structure and

including it in the three-dimension (3D) channel model, we were able to minimize the computing complexity of the 3D GBSM. To improve the functionality of the mMIMO CR-NOMA system, the RS employs a DF coding scheme to obtain results regarding achievable rate, outage probability, and bit-error rate through simulation. The main contribution this work are:

i. We determine the placement vector of the antenna element based on the physical structure of the antenna array to reduce the computational complexity of the model.

ii. We analyze a two-stage downlink mMIMO CR-NOMA system and offer a new 3D GBSM channel model when the transmitter is modelled as CA.

iii. We use DF coding scheme with the 3D channel model to improve on the performance of the mMIMO CR-NOMA system.

iv. For the two-stage CR-NOMA system's performance study, we report the outage probability, achievable rate and bit-error assessment. We compare these results with similar existing work that uses CBSM.

v. Results are shown to demonstrate the potential benefits of the joint contribution of large antenna transmitters and coding schemes using 3D GBSM model with mMIMO CR-NOMA to future communications systems in terms of achievable rate, outage probability, and bit-error rate (BER).

The paper is structured as follows. Section II gives the literature of prior work where the communication channel in the system is modeled as CBSM. It also establishes the motivation and contribution of the work. The proposed system model of the mMIMO CR-NOMA network and the proposed 3D GBSM model when the transmitter is cylindrical array (CA) is present in Section III. Sections IV and V contain the system's performance analysis, as well as numerical findings. Section VI concludes the paper, and state future works using 3D GBSM in NOMA and 5G systems.
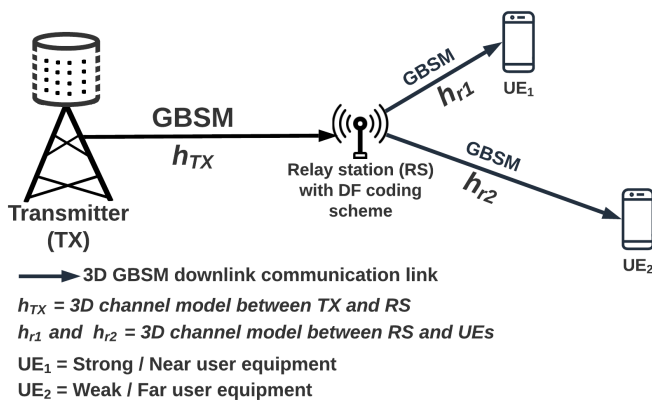

Fig. 3. Proposed Model of the Downlink Cooperative Relay NOMA Network with mMIMO.

III. System Model

As shown in *Fig.* 3, this section considers a two-stage downlink (DL) communication system in which the transmitter

(TX) transfers messages to user equipment (UE) via a dedicated relay. The TX has a large-scale antenna array such as CA for high spectral-efficient massive access, whereas the UEs and relay station (RS) each have a single antenna. Unlike the CR-NOMA model in *Fig.* 2, where the channel connecting the TX, RS, and UEs is modelled with CBSM, the proposed model substitutes the CBSM channel with a 3D GBSM, as illustrated in *Fig.* 3. The strong user equipment (UE$_1$) in the proposed system shown in *Fig.* 3 is located near to the RS, whereas the weak user equipment (UE$_2$) is located further away from the RS. We employ a fixed power allocations, and assign α_1 to UE$_1$, and α_2 to UE$_2$ according to NOMA principles where $\alpha_1 < \alpha_2$. TX combines the signal of the two UEs into one according to superposition principles. The combined signal ($\mathbf{x}$) of two is given by

$$\mathbf{x} = \sum_{i=1}^{2} \sqrt{\alpha_i} s_i \qquad (1)$$

where i^{th} user transmit power allocation and the source signal are α_i and s_i respectively. Noticeably $\sum_{i=1}^{2} \alpha_i \leq P_s$, where P_s is the total transmit power at TX. We assume that TX uses a pilot signal to estimate the downlink (DL) channel. Additionally, we take advantage of channel reciprocity using the traditional time division duplex mode [42]. The system uses two-time slots to transmit the combined signal to the user. During the first, the received signal (y) at the relay with DL data transmission is given by

$$y = \mathbf{H}\mathbf{x} + n \qquad (2)$$

where $\mathbf{x}$ is an $N_t \times 1$ data signal from (1), $\mathbf{H}$ is the channel matrix generated in (11) and n is the additive Gaussian white noise with zero mean and variance, σ^2.

A. Proposed 3D GBSM Models

We assess the GBSM-based 3GPP standard and offer a 3D channel model in which the TX antenna is treated as a CA. The main parameters of significance in the 3D channel model are the delay spread (DS), angle of arrival (AoA), azimuth of departure (AoD), the elevation angle of arrival, and elevation angle of departure [12], [43], [44].

Additionally, the proposed 3GPP standard allows for dynamic adaptation of the antenna's downtilt angles and the elevation angle of the boresight into the channel. According to [40], this offers several benefits for 3D beamforming, which can significantly boost system performance. *Fig.* 4 illustrates the 3D channel model, where the key parameters have been listed.

The effective channel between s^{th} TX antenna port with M subpath and u^{th} UE antenna port can be expressed as stated in [14], [39] as

$$\left[\mathbf{H}_{s,u}^{3D}\right] = \sqrt{\frac{P_n \sigma_{SF}}{M}} \sum_{n=1}^{N} \alpha_n \begin{bmatrix} \sqrt{G_{TX}^{3D}\left(\phi_n^{AoD}, \theta_n^{AoD}, \theta_{tilt}\right)} \\ \times \sqrt{G_{RS}^{3D}\left(\varphi_n^{AoA}, \vartheta_n^{AoA}\right)} \\ \times \left[a_{RX}\left(\varphi_n^{AoA}, \vartheta_n^{AoA}\right)\right]_u \\ \times \left[a_{TX}\left(\phi_n^{AoD}, \theta_n^{AoD}\right)\right]_s \end{bmatrix} \qquad (3)$$
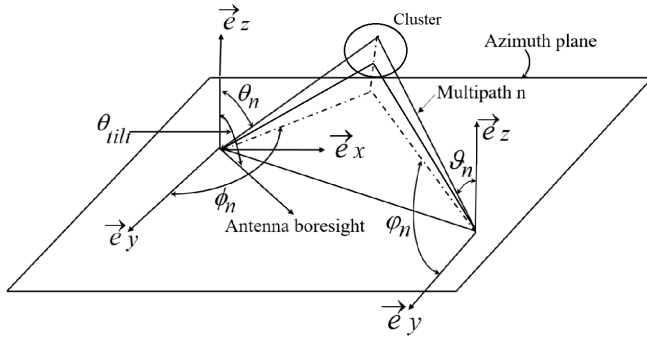
θ_{tilt} = Elevation angle of the boresight

θ_n, ϑ_n = Elevation AoD & AoA of the nth path respectively

ϕ_n, φ_n = Azimuth AoD & AoA of the nth path respectively

Fig. 4. 3D Channel Model.

where α_n is the complex random amplitude of the nth path. $s = 1,...,N_{TX}$, $u = 1,...,N_{RS}$, $(\phi_n^{AoD}, \theta_n^{AoD})$ are the azimuth and elevation angles-of-departure (AoD) respectively. $(a_{RX}(\varphi_n^{AoA}, \vartheta_n^{AoD}))$ and $(a_{TX}(\phi_n^{AoD}, \theta_n^{AoD}))$ are the antenna array response of transmitter and receiver antenna respectively. The azimuth and elevation AoA of the nth path respectively $(\varphi_n^{AoA}, \vartheta_n^{AoD})$, and θ_{tilt} are the downtilt angles of the antenna. The gain of the antenna array at the TX is $(\varphi_n^{AoA}, \vartheta_n^{AoA})$, and θ_{tilt}.

$$G_{TX}^{3D}\left(\phi_n^{AoD}, \theta_n^{AoD}, \theta_{tilt}\right) \approx G_{TX,H}\left(\phi_n^{AoD} G_{TX,V}(\theta_n, \theta_{tilt})\right) \tag{4}$$

where the G_{TX}^{3D} and G_{TX}^{3D} are given by the method in [14] and [45].

$$G_{TX,H}(\phi^{AoD}) = -12\left(\frac{\phi^{AoD}}{\phi_{3dB}}\right)^2 \tag{5}$$

and

$$G_{TX,V}(\theta^{AoD}, \theta_{tilt}) = -12\left(\frac{\theta^{AoD} - \theta_{tilt}}{\theta_{3dB}}\right)^2 \tag{6}$$

where ϕ^{AoD} is the azimuth angle between the user and the boresight of the array in the horizontal domain, θ^{AoD} is the elevation angle between the user and the boresight of the array in the vertical domain, φ_{3dB} and θ_{3dB} are the half-power beamwidth in horizontal and vertical domains, respectively. Equation (5) and (6) provide accurate 3D antenna radiation pattern in both the horizontal and vertical planes respectively.

We consider CA at the TX serving a single antenna RS and UEs with half duplex connection in this model. The path between TX and RS has a single bounce cluster giving us N number of paths. Using CA structure in *Fig.* 5, we consider the array dimension radius given by $\rho = 4\lambda/l$, where $l = 4\lambda$. If $d_z = 4\lambda/M$ is the wavelength distance in meters between the first and second antenna elements in the z direction, then $4\lambda(m-1)/M$ wavelengths may be used to estimate the placement of the third and fourth antenna components; where $m = 1,...,M$ is the number of antenna elements on a ring in the z-axis. λ is the wavelength in meters. The angular position

of the nth element of the mth of the CA on the *x-y* plane is

$$\varphi_s = 2\pi(n-1)/N \tag{7}$$

Consequently, the location vector of the elements can be expressed as

$$v_t \cdot x_s = \cos(\phi - \varphi_s)\sin\theta \tag{8}$$

Furthermore, the array response of sth transmit antenna port of the CA is given by

$$\left[a_{TX}(\phi_n^{AoD}, \theta_n^{AoD})\right]_s = \exp\left(\begin{array}{c} ik\rho\frac{4\lambda(m-1)}{M} \\ \times \cos(\phi_n - \varphi_s)\sin\theta_n^{AoD} \end{array}\right) \tag{9}$$

Similarly, the response of the uth UE antenna port with regards to the 3D channel model is

$$\left[a_{RX}(\varphi_n^{AoA}, \vartheta_n^{AoA})\right]_u = \exp\left(ik(u-1)d_r\sin\varphi\sin\vartheta\right) \tag{10}$$

Legend:
θ = Elevation angle
ϕ = Azimuth angle
ρ = Radius of the cylinder
d_z = Antenna element spacing in the z axis
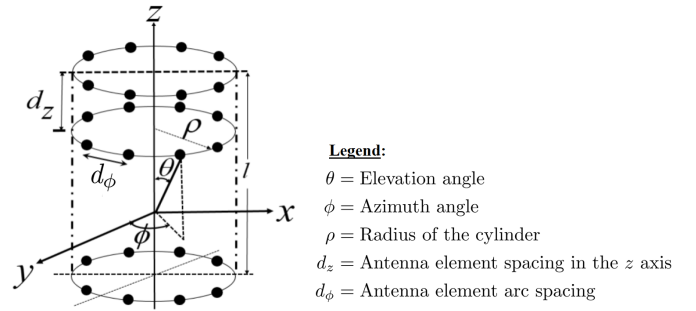d_ϕ = Antenna element arc spacing

Fig. 5. Cylindrical Array Geometric Structure.

The final 3D GBSM channel model [33], [46], [47] of the communication link in the proposed system in *Fig.* 3 between a single antenna receiving port u^{th} and a CA transmitter antenna port s^{th} [14] is

$$H_{s,u}^{CA} = \sqrt{\frac{P_n\sigma_{SF}}{M}}$$
$$\times \sum_{n=1}^{N}\alpha_n\left[\begin{array}{c} \sqrt{G_{TX}^{3D}\left(\phi_n^{AoD}, \theta_n^{AoD}, \theta_{tilt}\right)} \\ \times \exp\left(\begin{array}{c} ik\rho(4\lambda(m-1)/M) \\ \times \cos(\phi_n - \varphi_s)\sin\theta_n \end{array}\right) \\ \times \sqrt{G_{RS}^{RX}\left(\varphi_n^{AoA}, \vartheta_n^{AoA}\right)} \\ \times \exp\left(ik(u-1)d_r\sin\varphi\sin\vartheta\right) \end{array}\right] \tag{11}$$

IV. SYSTEM ANALYSIS

A. Transmission between TX and RS

We presented a 3D GBSM mMIMO CR-NOMA system model [46], [48] with large antenna transmitters such as CA, as shown in *Fig.* 3 The system model takes into consideration two fundamental presumptions. First of all, TX and UEs cannot directly communicate with one another. Second, in a half-duplex communication mode, users are outfitted with a single antenna. There are two phases to the communication between TX and UEs. During the first step, the TX sends a superposition of two unique signals (**x**) to the relay, which

relays it to all UEs after decoding. The received signal (y_{RS}) at the relay is

$$y_{RS} = \sqrt{\alpha_R} \mathbf{h}_{S,R} \mathbf{x} + \eta_R \tag{12}$$

where η_R is the additive white Gaussian noise (AWGN) with unit variance, $\mathbf{h}_{S,R}$ is the proposed 3D GBSM channel coefficient between the TX and RS presented in (11). The distance-dependent path loss, denoted by the expression α_R, depends on the distance between TX and RS and the path loss exponent. The use of the NOMA scheme necessitates that the power coefficients must be placed in the order $\alpha_1 < \alpha_2$, which corresponds to the channel gains.

B. Transmission between RS and UE

1) Application of DF Coding Scheme: The TX sends a superimposed signal to the relay during the first time slot in accordance with NOMA concepts. The achievable rates ($R_{x_1}^{\text{RS}}$ and $R_{x_2}^{\text{RS}}$) for the relay to decode x_1 and x_2 are given [49] by

$$R_{x_1}^{\text{RS}} = B\log_2\left(1 + \frac{\alpha_1 \gamma |\mathbf{h}_{S,R}|^2}{\alpha_2 \gamma |\mathbf{h}_{S,R}|^2 + 1}\right) \tag{13}$$

and

$$R_{x_2}^{\text{RS}} = B\log_2\left(1 + \alpha_2 \gamma |\mathbf{h}_{S,R}|^2\right) \tag{14}$$

where α_1 and α_2 are power allocation associated with x_1 and x_2 respectively.

Given that, the relay can decode the signal from the TX of the two NOMA users, the observable signal (y_k^{DF}) at UE_1 and UE_2 in the second slot may be stated as

$$y_k^{\text{DF}} = \mathbf{h}_{R,k} \sqrt{\beta_k} \mathbf{x} + \eta_k \tag{15}$$

where $k = 1, 2$ of users and $\beta_k > 0$ is the power allocation coefficient of the kth user, where $\beta_1 + \beta_2 = 1$.

Following the principle of NOMA scheme, the decoding order at the relay is $x_1 \rightarrow x_2$. The relay first detects x_1 by treating x_2 as noise. It then removes x_1 from the y_{RS} in (12) to detect x_2. By employing successive interference cancellation (SIC), the signal-to-interference ratio (SINR) ($\gamma_{1,2}^{\text{DF}}$) at UE_1 to detect x_2 is given [49] by

$$\gamma_{1,2}^{\text{DF}} = \frac{\beta_2 \gamma |\mathbf{h}_{R,1}|^2}{\beta_1 \gamma |\mathbf{h}_{R,1}|^2 + 1} \tag{16}$$

The SINR ($\gamma_{R,1}^{\text{DF}}$) for UE_1 to detect its own signal is given by

$$\gamma_{R,1}^{\text{DF}} = \beta_1 \gamma |\mathbf{h}_{R,1}|^2 \tag{17}$$

Similarly, the SINR ($\gamma_{R,2}^{\text{DF}}$) at UE_2 is given [49] by

$$\gamma_{R,2}^{\text{DF}} = \frac{\beta_2 \gamma |\mathbf{h}_{R,2}|^2}{\beta_1 \gamma |\mathbf{h}_{R,2}|^2 + 1} \tag{18}$$

C. Achievable Rates Analysis

The system's maximum achievable rate in the channel is when the BER goes to zero. The achievable rates of UEs may be determined based on the SINR values when the CSI is unknown at the transmitter with independent equi-powered transmissions. With regards to DF coding scheme, the achievable rates at the destination nodes from (16)–(18) are given by

$$\begin{aligned} R_{UE_1}^{\text{DF}} &= \min[R_{x_1}^{\text{RS}}, B\log_2(1 + \gamma_{R,1}^{\text{DF}})] \quad \text{and} \\ R_{UE_2}^{\text{DF}} &= \min[R_{x_2}^{\text{RS}}, B\log_2(1 + \gamma_{R,2}^{\text{DF}})] \end{aligned} \tag{19}$$

The relay transmits the decoded signals to all UEs during the second time slot.

D. Outage Probabilities Analysis

To estimate the possibility of an outage event occurring in a data stream where the achievable data rate is lower than the encoded data rate [20], [50], we investigate the outage probability when the UE_1 is capable of detecting x_2 and x_1. The outage probability (P_1) of UE_1 in relation to the threshold signal-to-noise ratio (SNR) for CR-NOMA users UE_1, UE_2 (denoting Ω_1, Ω_2, respectively) may be characterized as follows based on the preceding definition:

$$\begin{aligned} P_1 &= \left[1 - P_r(\xi_{\text{RS}} \geq \xi'_{\Omega_2}, \xi_{\text{RS}} \geq \xi'_{\Omega_1})\right] \\ &\times \left[1 - P_r(\xi_{l,2}^{\text{DF}} \geq \xi'_{\Omega_2}, \xi_1^{\text{DF}} \geq \xi'_{\Omega_1})\right] \end{aligned} \tag{20}$$

where $\xi'_{\Omega_1} = 2^{2\tilde{\mathcal{R}}_1} - 1$ and $\xi'_{\Omega_2} = 2^{2\tilde{\mathcal{R}}_2} - 1$ are the decoding threshold with $\tilde{\mathcal{R}}_1$ and $\tilde{\mathcal{R}}_2$ being the target rate of UE_1 and UE_2 respectively. ξ_{RS} is the SINR between TX and RS, ξ_{RS} is the decoding threshold of the direct transmission to the RS. ξ_1^{DF} and ξ_2^{DF} are the SINR defined at (17) and (18). Similarly, the outage probability (P_2) of UE_2 can be expressed as

$$P_2 = P_r(\xi_{\text{RS}} < \xi'_{\Omega_2}, \ \xi_2^{\text{DF}} < \xi'_{\Omega_2}) \tag{21}$$

E. Bit-Error Rates Analysis

We provide the bit-error analysis for the proposed CR-NOMA system in accordance with the recommendations in the [51]. According to [51], the average percentage error ($P_e^{\text{UE}_1}$) of the UE_1 under the assumption that its symbols are successfully and mistakenly recognized by using SIC processing is

$$\begin{aligned} P_e^{\text{UE}_1} &= \frac{1}{2}\left(1 - \sqrt{\frac{\gamma_{\mathcal{B}_1}}{2 + \gamma_{\mathcal{B}_1}}}\right) \\ &+ \frac{1}{8}\left[\sqrt{\frac{\gamma_{\mathcal{B}_2}}{2 + \gamma_{\mathcal{B}_2}}} - \sqrt{\frac{\gamma_{\mathcal{B}_3}}{2 + \gamma_{\mathcal{B}_3}}} \right. \\ &\left. + \sqrt{\frac{\gamma_{\mathcal{B}_4}}{2 + \gamma_{\mathcal{B}_4}}} - \sqrt{\frac{\gamma_{\mathcal{B}_5}}{2 + \gamma_{\mathcal{B}_5}}}\right] \end{aligned} \tag{22}$$

where, for various constellation points of x_1 and x_2, the SNRs are provided by with signal energies (ε_1, ε_2).

$$\gamma_{\mathcal{B}_1} = \frac{\varepsilon_1}{N_0} E\left[|\mathbf{h}_{R,1}|^2\right]$$

$$\gamma_{\mathcal{B}_2} = \frac{\left(\sqrt{2\varepsilon_2} + \sqrt{\varepsilon_1}\right)^2}{N_0} E\left[|\mathbf{h}_{R,1}|^2\right] \tag{23}$$

$$\gamma_{\mathcal{B}_3} = \frac{\left(\sqrt{2\varepsilon_2} - \sqrt{\varepsilon_1}\right)^2}{N_0} E\left[|\mathbf{h}_{R,1}|^2\right]$$

and

$$\gamma_{\mathcal{B}_4} = \frac{\left(2\sqrt{2\varepsilon_2} + \sqrt{\varepsilon_1}\right)^2}{N_0} E\left[|\mathbf{h}_{R,1}|^2\right]$$
$$\gamma_{\mathcal{B}_5} = \frac{\left(2\sqrt{2\varepsilon_2} - \sqrt{\varepsilon_1}\right)^2}{N_0} E\left[|\mathbf{h}_{R,1}|^2\right] \quad (24)$$

Equation (24) reflects the circumstance in which UE_1 is unable to detect its signals properly, whereas (23) describes the circumstance in which the signals are successfully detected. Comparably, the UE_2's overall average BER ($P_e^{UE_2}$) performance from citation [51] is

$$P_e^{UE_2} = \frac{1}{4}\left[\left(1 - \sqrt{\frac{\gamma_{\mathcal{A}_1}}{2 + \gamma_{\mathcal{A}_1}}}\right) + \left(1 - \sqrt{\frac{\gamma_{\mathcal{A}_2}}{2 + \gamma_{\mathcal{A}_2}}}\right)\right] \quad (25)$$
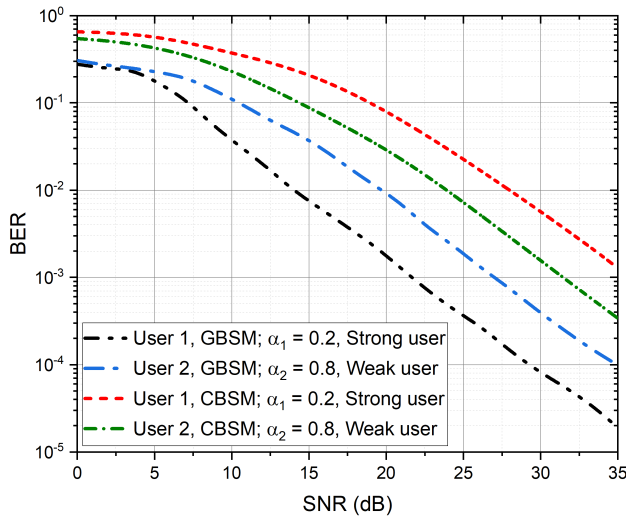
Fig. 6. BER of DF Schemes of the Proposed 3D Channel Model with CA.

where $\gamma_{\mathcal{A}_1}$ and $\gamma_{\mathcal{A}_2}$ are the SNRs of different signal constellation points expressed as

$$\gamma_{\mathcal{A}_1} = \frac{\left(\sqrt{2\varepsilon_2} + \sqrt{\varepsilon_1}\right)^2}{N_0} E\left[|\mathbf{h}_{R,2}|^2\right],$$
$$\gamma_{\mathcal{A}_2} = \frac{\left(\sqrt{2\varepsilon_2} - \sqrt{\varepsilon_1}\right)^2}{N_0} E\left[|\mathbf{h}_{R,2}|^2\right] \quad (26)$$

V. NUMERICAL RESULTS AND DISCUSSION

In this section, we validate the proposed 3D channel model for mMIMO CR-NOMA applications using simulation and numerical assessment. By setting the AoA cluster to 0.7 and the AoA offset standard deviations to $(\sigma_{\Delta_\phi}, \sigma_{\Delta_\theta})$ at 2.6 GHz carrier frequency, we are able to analyze the proposed 3D GBSM models. Adjacent antenna elements on the z axis are separated by $l = 4\lambda$ and are situated at a maximum radius of $\rho = 2\pi/l$ from the cylinder centre with respect to the x, y plane. There were two circular arrays in the azimuth domain, each with $N_t = 4$ elements, making up the $2 \times N_t$ number of elements of the CA. Summary of other simulation parameters is listed in *Table* II

For the TX antenna topology, we calculated the channel coefficient based on the channel realization between the sth

TABLE II. 3D GBSM CR-NOMA MMIMO SIMULATION PARAMETERS

Parameter	Value
Frequency	2.6 GHz
$\theta_t ilt$	$95°$
θ_3dB	$15°$
ϕ_3dB	$70°$
Number of clusters	1
Number of users	2
Path-loss exponent	4
Environment	Urban Macrocell
Fixed power allocation	$\alpha_1 = 0.3$, $\alpha_2 = 0.7$

transmit antenna port and uth receive antenna port. $\theta_{tilt} = 95°$, $\theta_{3dB} = 15°$ and $\phi_{3dB} = 70°$ were taken into consideration to validate the proposed model for the 3D channel modeling from the TX to UEs through RS in *Fig.* 3. Furthermore, the 3GPP-specified Laplacian distributions are used to describe the power of the azimuth spectrum reaching the RS, multipath components for each AoA, and the multipath delay related to each AoD. We examined the DF in conjunction with the 3D GBSM channel. The outage probability (OP), achievable rate and BER are calculated for the DF coding scheme of *Fig.* 2 and compared with the outcomes of a system using theoretical channel models such as CBSM throughout.
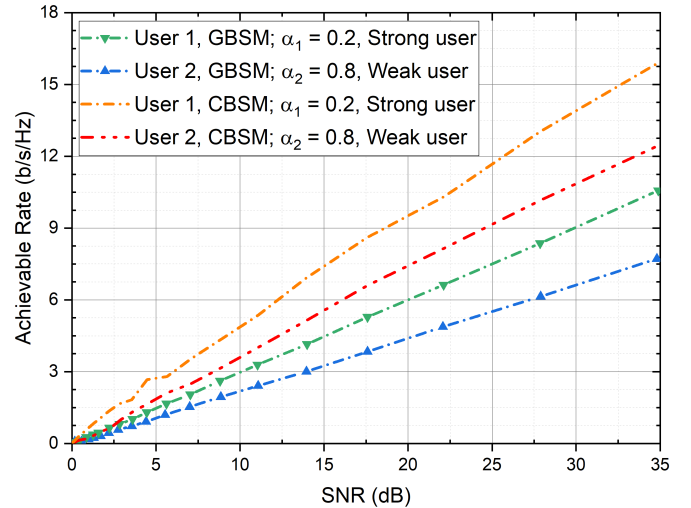

Fig. 7. Achievable Rates of DF of the Proposed 3D Channel Model with CA.

A. BER Performance

The channel coefficients between both the transmitter and the relay have been produced using (11), respectively, for BER performance evaluation. Using (22) and (25), respectively, the BER of UE_1 and UE_2 was calculated. The BER for different SNR values in dB for the proposed 3D GBSM channel model of CA uses 68 antenna components is shown in *Figs.* 6.

In *Fig.* 6, the performance of UE_1 is better than that of UE_2, which is owing to the fact that UE_1 is closer to the RS and has a good channel condition than that of UE_2. It should be noted that 3D GBSM models have high computational complexity with unpredictability parameters which could affect

TABLE III. COMPARISON OF OP AND BER WITH PRIOR WORKS AT SNR OF 20 dB

Ref	Antenna Type	No. of Users	BER	OP
Proposed	Multiple antenna TX, single antenna RS and UE	2	$10^{-2.85}$	$10^{-2.50}$
[20]	Single antenna TX, RS and UE	2	$10^{-2.10}$	$10^{-1.50}$
[52]	Single antenna TX, RS and UE	2	-	$10^{-0.80}$
[53]	Single antenna TX, RS and UE	1	$10^{-2.70}$	-
[54]	Single antenna TX, RS and UE	2	$10^{-4.96}$	-
[55]	Multiple antenna TX, single antenna RS and UE	1	-	$10^{-2.45}$
[56]	Multiple antenna TX, UE, single antenna RS	1	-	$10^{-0.28}$

the performance of the system. However, our results on the BER using DF coding strategy at 20 dB are comparable to prior works done in the literature that employs the CBSM channel models (*Table* III). This may be due to the use of the antenna element placement vector, which we defined based on the physical structure of the antenna as described in *Fig.* 5. *Table* III compares the proposed system's outage probability and BER performance to previous research studies that employ the CBSM channel model which confirms the results of *Fig.* 6. Except for [52], which contains M relays, all other references including the proposed system employ a single relay device.
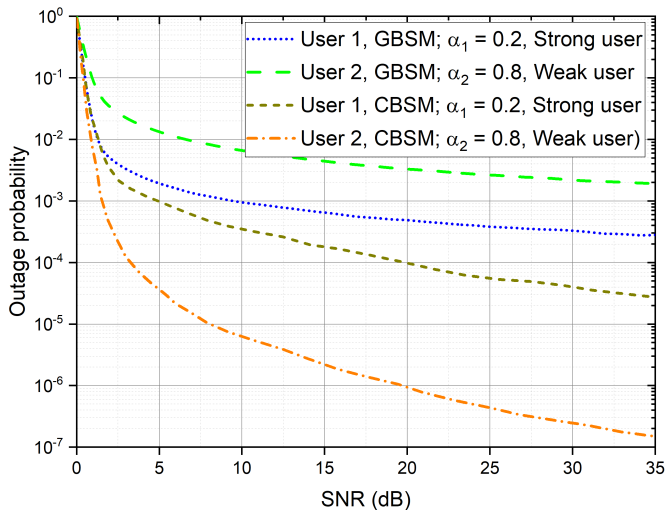

Fig. 8. Comparison of OP of Two Users using DF Scheme of the Proposed Channel Models with CA.

In contrast to GBSM, which has high computational complexity, a high proportion of random propagation, and channel parameters like path-loss, delay profile, tilt angle, angle of arrival, angle of departure, etc. that reflect realistic and practical mMIMO systems, CBSM is primarily used for link-level simulation and to analyze the theoretical performance of mMIMO systems. Consequently, CBSM performance is

superior to GBSM as indicated in *Table* III and the figures above.

B. Achievable Rate and Outage Probability Performances

Equation (19) calculates the achievable rates of DF for the achievable rate analysis. In *Fig.* 7, the achievable rate of using DF coding scheme shows considerable improvement as compared with the results of CBSM. We demonstrate the outage performance of the proposed system as a function of transmit SNR in *Fig.* 8 by using 3D GBSM channel model with CA in (11). The performance differences between two users, UE_1 and UE_2, extends over the entire SNR range. The system outage performance may be significantly improved by changing the transmitter array configuration, increasing the TX's antenna capacity, and maintaining a single antenna at the relay node. Furthermore, it reveals that UE_2 has a worse outage than UE_1. This is expected since further from the RS than UE_1, and therefore, it has poor channel condition.

Again, the system uses less transmit power at the relay for RS–UEs links to process the second-hop signal, which decreases the performance of the hop's outage. *Fig.* 8 gives the outage probability of the two users using the 3D GBSM channel and the DF relay coding strategy. It can be demonstrated that the OP of the DF coding scheme performs better with the 3D GBSM channel model.

VI. CONCLUSION AND FUTURE WORK

We provided a 3D GBSM channel model between TX–RS and TX–UEs in this study. We investigated a two-stage mMIMO CR-NOMA downlink system with a 3D GBSM channel model, where the transmitter is represented by CA. We defined the antenna placement vector based on the physical structure of the antenna design to reduce the computational complexity of the channel. For improved channel performance, the proposed 3D GBSM channel model uses a DF network coding scheme. For the two-stage system, we calculated the probability of an outage, the achievable rate, and the BER. In terms of outage probability, attainable rate, and other crucial network performance parameters, integrating NOMA with cooperative relay transmission mechanism guarantees a notable boost to the performance of the 5G networks. The outage probability of cooperative relay integrated NOMA over a 3D GBSM channel is explored in this work. Lastly, despite the fact that the proposed 3D GBSM channel model has a greater computational cost in terms of complexity, the results show that the differences in performance between CBSM and GBSM channel models are marginal. The marginal performance of CBSM over the GBSM model is due to the channel model's lower computing complexity and less random channel parameters, which makes it suitable for theoretical analysis of mMIMO systems. The research may be expanded to include millimetre-wave CR-NOMA with multiple antennas at the TX, RS, and UE. The influence of spatial correlation of antenna array arrangement on 3D GBSM performance in CR-NOMA system may be explored for certain applications such as high-speed train communication, unmanned aerial vehicle, the vast internet of things, and so on.

REFERENCES

[1] M. W. Akhtar, S. A. Hassan, R. Ghaffar, H. Jung, S. Garg, and M. S. Hossain, "The shift to 6g communications: vision and requirements," *Human-centric Computing and Information Sciences*, vol. 10, no. 1, pp. 1–27, 2020.

[2] I. Rosaline, A. Kumar, P. Upadhyay, and A. H. Murshed, "Four element mimo antenna systems with decoupling lines for high-speed 5g wireless data communication," *International Journal of Antennas and Propagation*, vol. 2022, 2022.

[3] A. Al-Ansi, A. M. Al-Ansi, A. Muthanna, I. A. Elgendy, and A. Koucheryavy, "Survey on intelligence edge computing in 6g: Characteristics, challenges, potential use cases, and market drivers," *Future Internet*, vol. 13, no. 5, p. 118, 2021.

[4] O. Omarov, G. Nauryzbayev, S. Arzykulov, M. S. Hashmi, and A. M. Eltawil, "Capacity analysis of wireless powered cooperative noma networks over generalized fading," in *2021 IEEE Wireless Communications and Networking Conference (WCNC)*. IEEE, 2021, pp. 1–6.

[5] A. Al Amin and S. Y. Shin, "Capacity analysis of cooperative noma-oam-mimo based full-duplex relaying for 6g," *IEEE Wireless Communications Letters*, vol. 10, no. 7, pp. 1395–1399, 2021.

[6] I. Budhiraja, N. Kumar, S. Tyagi, S. Tanwar, Z. Han, D. Y. Suh, and M. J. Piran, "A systematic review on noma variants for 5g and beyond," *IEEE Access*, 2021.

[7] S. R. Islam, M. Zeng, O. A. Dobre, and K.-S. Kwak, "Resource allocation for downlink noma systems: Key techniques and open issues," *IEEE Wireless Communications*, vol. 25, no. 2, pp. 40–47, 2018.

[8] A. Akbar, S. Jangsher, and F. A. Bhatti, "Noma and 5g emerging technologies: A survey on issues and solution techniques," *Computer Networks*, vol. 190, p. 107950, 2021.

[9] L. Han, R. Liu, Z. Wang, X. Yue, and J. S. Thompson, "Millimeter-wave mimo-noma-based positioning system for internet-of-things applications," *IEEE Internet of Things Journal*, vol. 7, no. 11, pp. 11 068–11 077, 2020.

[10] E. J. Oughton, W. Lehr, K. Katsaros, I. Selinis, D. Bubley, and J. Kusuma, "Revisiting wireless internet connectivity: 5g vs wi-fi 6," *Telecommunications Policy*, vol. 45, no. 5, p. 102127, 2021.

[11] R. Shankar, "Examination of a non-orthogonal multiple access scheme for next generation wireless networks," *The Journal of Defense Modeling and Simulation*, vol. 19, no. 3, pp. 453–465, 2022.

[12] K. Zheng, S. Ou, and X. Yin, "Massive mimo channel models: A survey," *International Journal of Antennas and Propagation*, vol. 2014, 2014.

[13] P. Zhang, J. Chen, X. Yang, N. Ma, and Z. Zhang, "Recent research on massive mimo propagation channels: A survey," *IEEE Communications Magazine*, vol. 56, no. 12, pp. 22–29, 2018.

[14] A. E. Ampoma, G. Wen, Y. Huang, K. O. Gyasi, P. I. Tebe, and K. Ntiamoah-Sarpong, "Spatial correlation models of large-scale antenna topologies using maximum power of offset distribution and its application," *IEEE Access*, vol. 6, pp. 36 295–36 304, 2018.

[15] K. Zheng, L. Zhao, J. Mei, B. Shao, W. Xiang, and L. Hanzo, "Survey of large-scale mimo systems," *IEEE Communications Surveys & Tutorials*, vol. 17, no. 3, pp. 1738–1760, 2015.

[16] D. He, B. Ai, K. Guan, L. Wang, Z. Zhong, and T. Kürner, "The design and applications of high-performance ray-tracing simulation platform for 5g and beyond wireless communications: A tutorial," *IEEE Communications Surveys & Tutorials*, vol. 21, no. 1, pp. 10–27, 2018.

[17] S. Joshi and M. S. Bhakta, "Power efficient multi-relay cooperative diversity in wireless network using hybrid relaying protocol," in *Future of Information and Communication Conference*. Springer, 2020, pp. 60–78.

[18] M. B. Uddin, M. F. Kader, and S. Y. Shin, "Cooperative relaying using mimo noma," in *2018 4th international conference on wireless and telematics (ICWT)*. IEEE, 2018, pp. 1–6.

[19] M. Liaqat, K. A. Noordin, T. A. Latef, and K. Dimyati, "Power-domain non orthogonal multiple access (pd-noma) in cooperative networks: an overview," *Wireless Networks*, vol. 26, no. 1, pp. 181–203, 2020.

[20] K. Ntiamoah-Sarpong, Z. Huang, G. Wen, and A. E. Ampoma, "Performance of non-orthogonal multiple access: analysis using compute-and-forward cooperative relaying in 5g networks," *IET Communications*, vol. 14, no. 17, pp. 3058–3064, 2020.

[21] M. Zeng, W. Hao, O. A. Dobre, and Z. Ding, "Cooperative noma: State of the art, key techniques, and open challenges," *IEEE Network*, vol. 34, no. 5, pp. 205–211, 2020.

[22] V. Goutham and V. Harigovindan, "Full-duplex cooperative relaying with noma for the performance enhancement of underwater acoustic sensor networks," *Engineering Science and Technology, an International Journal*, 2021.

[23] J. Sushma, M. N. Gayathri, S. Srivani, V. N. Nayak, and K. K. Gurrala, "Performance analysis and power allocation for multi relay wireless cooperative noma networks with diversity combining strategies," in *2020 IEEE International Students' Conference on Electrical, Electronics and Computer Science (SCEECS)*. IEEE, 2020, pp. 1–6.

[24] G. Li, D. Mishra, Y. Hu, Y. Huang, and H. Jiang, "Adaptive relay selection strategies for cooperative noma networks with user and relay cooperation," *IEEE Transactions on Vehicular Technology*, vol. 69, no. 10, pp. 11 728–11 742, 2020.

[25] Z. Zhang and Z. Si, "Performance evaluation and optimization of cooperative noma over rayleigh fading channels," in *2020 IEEE International Conference on Communications Workshops (ICC Workshops)*. IEEE, 2020, pp. 1–6.

[26] H. Wang, R. Shi, K. Tang, J. Dong, and S. Liao, "Performance analysis and optimization of a cooperative transmission protocol in noma-assisted cognitive radio networks with discrete energy harvesting," *Entropy*, vol. 23, no. 6, p. 785, 2021.

[27] G. Alnwaimi, H. Boujemaa, and K. Arshad, "Throughput optimization of cooperative non orthogonal multiple access," *Telecommunication Systems*, vol. 76, no. 3, pp. 359–370, 2021.

[28] K. Reshma and A. Babu, "Cooperative noma system with incremental relaying and energy harvesting: Performance analysis and optimization," *Transactions on Emerging Telecommunications Technologies*, vol. 31, no. 9, p. e4075, 2020.

[29] A. Nazari, M. R. Javan, and S. S. Hosseini, "Resource allocation in power domain noma-based cooperative multicell networks." *IET Commun.*, vol. 14, no. 7, pp. 1162–1168, 2020.

[30] A. Rezaei, P. Azmi, N. M. Yamchi, M. R. Javan, and H. Yanikomeroglu, "Robust resource allocation for cooperative miso-noma-based heterogeneous networks," *IEEE Transactions on Communications*, vol. 69, no. 6, pp. 3864–3878, 2021.

[31] J. Kaur and M. L. Singh, "User assisted cooperative relaying in beamspace massive mimo noma based systems for millimeter wave communications," *China Communications*, vol. 16, no. 6, pp. 103–113, 2019.

[32] X. Chen, R. Jia, and D. W. K. Ng, "The application of relay to massive non-orthogonal multiple access," *IEEE Transactions on Communications*, vol. 66, no. 11, pp. 5168–5180, 2018.

[33] T. Zhou, Y. Yang, L. Liu, C. Tao, and Y. Liang, "A dynamic 3-d wideband gbsm for cooperative massive mimo channels in intelligent high-speed railway communication systems," *IEEE Transactions on Wireless Communications*, 2020.

[34] G. Li and D. Mishra, "Cooperative noma networks: User cooperation or relay cooperation?" in *ICC 2020-2020 IEEE International Conference on Communications (ICC)*. IEEE, 2020, pp. 1–6.

[35] R. R. Kurup, S. Mahin, M. Sandhyana, V. Priyanka, A. Babu *et al.*, "Outage performance of cooperative noma system in log-normal fading channels," in *2020 IEEE International Conference on Electronics, Computing and Communication Technologies (CONECCT)*. IEEE, 2020, pp. 1–6.

[36] M. Aldababsa and O. Kucur, "Outage and ergodic sum-rate performance of cooperative mimo-noma with imperfect csi and sic," *International Journal of Communication Systems*, vol. 33, no. 11, p. e4405, 2020.

[37] A. L. Imoize, A. E. Ibhaze, A. A. Atayero, and K. Kavitha, "Standard propagation channel models for mimo communication systems," *Wireless Communications and Mobile Computing*, vol. 2021, 2021.

[38] T. Zugno, M. Polese, N. Patriciello, B. Bojović, S. Lagen, and M. Zorzi, "Implementation of a spatial channel model for ns-3," in *Proceedings of the 2020 Workshop on ns-3*, 2020, pp. 49–56.

[39] Q.-U.-A. Nadeem, A. Kammoun, M. Debbah, and M.-S. Alouini, "Spatial correlation characterization of a uniform circular array in 3d mimo systems," in *2016 IEEE 17th International Workshop on Signal Processing Advances in Wireless Communications (SPAWC)*, 2016, pp. 1–6.

[40] A. Kammoun, M. Debbah, M.-S. Alouini *et al.*, "3d massive mimo systems: Modeling and performance analysis," *IEEE Transactions on wireless communications*, vol. 14, no. 12, pp. 6926–6939, 2015.

[41] L. Bai, Z. Huang, Y. Li, and X. Cheng, "A 3d cluster-based channel model for 5g and beyond vehicle-to-vehicle massive mimo channels," *IEEE Transactions on Vehicular Technology*, vol. 70, no. 9, pp. 8401–8414, 2021.

[42] E. Björnson, J. Hoydis, M. Kountouris, and M. Debbah, "Massive mimo systems with non-ideal hardware: Energy efficiency, estimation, and capacity limits," *IEEE Transactions on information theory*, vol. 60, no. 11, pp. 7112–7139, 2014.

[43] K. Guan, D. He, B. Ai, Y. Chen, C. Han, B. Peng, Z. Zhong, and T. Kuerner, "Channel characterization and capacity analysis for thz communication enabled smart rail mobility," *IEEE Transactions on Vehicular Technology*, vol. 70, no. 5, pp. 4065–4080, 2021.

[44] K. Guan, B. Ai, D. He, F. Zhu, H. Yi, J. Dou, and Z. Zhong, "Channel sounding and ray tracing for thz channel characterization," in *2020 13th UK-Europe-China Workshop on Millimetre-Waves and Terahertz Technologies (UCMMT)*. IEEE, 2020, pp. 1–3.

[45] J. Meredith, "Study on channel model for frequency spectrum above 6 ghz," *3GPP TR 38.900, Jun, Tech. Rep.*, 2016.

[46] Y. Zheng, L. Yu, R. Yang, and C.-X. Wang, "A general 3d non-stationary massive mimo gbsm for 6g communication systems," in *2021 IEEE Wireless Communications and Networking Conference (WCNC)*. IEEE, 2021, pp. 1–6.

[47] W. Zeng, Y. He, B. Li, and S. Wang, "3d multiple-antenna channel modeling and propagation characteristics analysis for mobile internet of things," *Sensors*, vol. 21, no. 3, p. 989, 2021.

[48] Y. Xie, B. Li, X. Zuo, M. Yang, and Z. Yan, "A 3d geometry-based stochastic model for 5g massive mimo channels," in *2015 11th International Conference on Heterogeneous Networking for Quality, Reliability, Security and Robustness (QSHINE)*. IEEE, 2015, pp. 216–222.

[49] Z. Wang, Z. Peng, Y. Pei, and H. Wang, "Performance analysis of cooperative noma systems with incremental relaying," *Wireless Communications and Mobile Computing*, vol. 2020, 2020.

[50] Z. Zhang, P. Dong, X. Tan, Y. Li, and K. Xiong, "Outage performance of wireless powered decode-and-forward relaying networks in rician fading," *Entropy*, vol. 24, no. 6, p. 763, 2022.

[51] F. Kara and H. Kaya, "Ber performances of downlink and uplink noma in the presence of sic errors over fading channels," *IET Communications*, vol. 12, no. 15, pp. 1834–1844, 2018.

[52] Z. Yang, Z. Ding, Y. Wu, and P. Fan, "Novel relay selection strategies for cooperative noma," *IEEE Transactions on Vehicular Technology*, vol. 66, no. 11, pp. 10 114–10 123, 2017.

[53] X. Wu and L.-L. Xie, "On the optimal compressions in the compress-and-forward relay schemes," *IEEE Transactions on Information Theory*, vol. 59, no. 5, pp. 2613–2628, 2013.

[54] Q. Li, M. Wen, E. Basar, H. V. Poor, and F. Chen, "Spatial modulation-aided cooperative noma: Performance analysis and comparative study," *IEEE Journal of Selected Topics in Signal Processing*, vol. 13, no. 3, pp. 715–728, 2019.

[55] T. M. Hoang, B. C. Nguyen, X. N. Tran, and L. T. Dung, "Outage probability and ergodic capacity of user clustering and beamforming mimo-noma relay system with imperfect csi over nakagami-m fading channels," *IEEE Systems Journal*, pp. 1–12, 2020.

[56] C.-B. Le, D.-T. Do, and M. Voznak, "Wireless-powered cooperative mimo noma networks: Design and performance improvement for cell-edge users," *Electronics*, vol. 8, no. 3, p. 328, 2019.